WATER RESOURCES RESEARCH, VOL. 49, 291–305, doi:10.1029/2012WR012755, 2013

A stochastic reconstruction framework for analysis of water resource system vulnerability to climate-induced changes in river flow regime

Alireza Nazemi,[1] Howard S. Wheater,[2] Kwok P. Chun,[3] and Amin Elshorbagy[4]

Received 1 August 2012; revised 13 October 2012; accepted 26 November 2012; published 24 January 2013.

[1] Assessments of potential impacts of climate change on water resources systems are generally based on the use of downscaled climate scenarios to force hydrological and water resource systems models and hence quantify potential changes in system response. This approach, however, has several limitations. The uncertainties in current climate and hydrological models can be large, such analyses are rapidly outdated as new scenarios become available, and limited insight into system response is obtained. Here, we propose an alternative methodology in which system vulnerability is analyzed directly as a function of the potential variations in flow characteristics. We develop a stochastic reconstruction framework that generates a large ensemble of perturbed flow series at the local scale to represent a range of potential flow responses to climate change. From a theoretical perspective, the proposed reconstruction scheme can be considered as an extension of both the conventional resampling and the simple *delta*-methods. By the use of a two-parameter representation of regime change (i.e., the shift in the timing of the annual peak and the shift in the annual flow volume), system vulnerability can be visualized in a two-dimensional map. The methodology is applied to the current water resource system in southern Alberta, Canada, to explore the system's vulnerability to potential changes in the streamflow regime. Our study shows that the system is vulnerable to the expected decrease in annual flow volume, particularly when it is combined with an earlier annual peak. Under such conditions, adaptation will be required to return the system to the feasible operational mode.

Citation: Nazemi, A., H. S. Wheater, K. P. Chun, and A. Elshorbagy (2013), A stochastic reconstruction framework for analysis of water resource system vulnerability to climate-induced changes in river flow regime, *Water Resour. Res.*, *49*, doi: 10.1029/2012WR012755.

1. Introduction

[2] For most water resource systems, performance is highly dependent on the natural flow regime. This is particularly the case in snow-dominated regions [*Barnett et al*., 2005], where snowmelt runoff is the predominant source of the water resources. Changes to the flow regime are thus of major concern, especially in western Canada, where increasing temperatures over recent decades have affected the snowpack and glacial storage and changed the variability and the form of precipitation [e.g., *Déry et al*., 2009]. These changes are typically reflected in the annual flow hydrographs in terms of earlier and less intense peak flow as well as decreased flow volume, particularly during summer [e.g., *Déry* and *Wood*, 2005]. The response of water resources systems to these changes can be quite dramatic, especially in semiarid cold regions such as the Canadian prairies. The Canadian prairies historically receive low and extremely variable annual precipitation and rely on runoff from the Canadian Rocky Mountains to support high surface water demand from major agricultural and municipal users in the basin [e.g., *Lemman* and *Warren*, 2004; *Martz et al*., 2007]. These characteristics make the Canadian prairies highly vulnerable to changes in the flow regime as the result of climate change.

[3] Most assessments of the response of water resources systems to climate change are based on using downscaled climate scenarios from one or more global or regional climate models to force hydrological models and thus to predict the flow regime change [e.g., *Minville et al*., 2009; *Viviroli et al*. 2010; *Hall* and *Murphy*, 2010]. The projected flow series are then presented to water resources systems simulation models to determine the system response. There are, however, several criticisms of this stereotypical pathway. There is widespread recognition that global climate model

[1]Global Institute for Water Security and the Department of Civil and Geological Engineering, National Hydrology Research Centre, University of Saskatchewan, Saskatoon, Saskatchewan, Canada.
[2]CERC in Water Security, National Hydrology Research Centre, University of Saskatchewan, Saskatoon, Saskatchewan, Canada.
[3]Global Institute for Water Security and School of Environment and Sustainability, National Hydrology Research Centre, University of Saskatchewan, Saskatoon, Saskatchewan, Canada.
[4]Civil and Geological Engineering and Global Institute for Water Security, University of Saskatchewan, Saskatoon, Saskatchewan, Canada.

Corresponding author: A. Nazemi, Global Institute for Water Security, University of Saskatchewan, National Hydrology Research Centre, 11 Innovation Boulevard, Saskatoon SK S7N 3H5, Canada (ali.nazemi@usask.ca)

0043-1397/13/2012WR012755

(GCM) and regional climate model have major limitations, in particular with respect to the representation of precipitation [e.g., *Leith* and *Chandler*, 2010; *Anagnostopoulos et al*., 2010]. *Kundzewiz et al*. [2007] presented results for the Intergovernmental Panel on Climate Change Fourth Assessment Report, using an ensemble of climate models, which show many areas of the world in which not only the magnitude but also the sign of change in future precipitation is uncertain. In addition, *Kundzewiz* and *Stakhiv* [2010] argued that the current generation of GCMs does not contain the detail required for water security studies and that significant improvements are required before GCMs can be directly used in water resource planning and management.

[4] Several authors have also warned about the additional uncertainty in hydrological modeling. *Beven* [2008, 2011] argued that several factors add a great deal of uncertainty to future hydrological projections. These include (1) possible variations in parameters of hydrological models due to the nonstationary climate, (2) gaps in process representations, (3) the issue of parametric identifiability, and (4) the grand challenge of prediction in ungauged basins. *Wilby* [2010] argued that, even if perfect climate and hydrological models were to exist, the uncertainties in future land use, human behavior, economy, governance, and other forcings make any quantification highly uncertain. Moreover, there are huge concerns about how the public and policy makers perceive the scientific outcomes from climate and hydrological models [e.g., *Budescu et al*., 2009; *Swart et al*., 2008]. *Stedman* [2004] noted that results of climate models do not have a strong influence on the perception of the risk associated with climate change, even for key policy makers. *Wheater* [2009] argued that development of adaptation strategies that acknowledge such scientific and social complexities is a priority in vulnerability assessment of water resources systems under changing climate. *Pielke* and *Wilby* [2012] discussed that vulnerability of water resources systems can be due to a wide spectrum of natural and social forces. They suggested that, at this stage, a general framework is required to assign the coping conditions under which the system is resilient to the potential change, as well as critical thresholds, beyond which any further change causes harm to the water resources systems.

[5] Because of these issues, it seems that a more general assessment is required to address the vulnerability of water resources systems to possible changes in the flow regime than that projected using climate and/or hydrological models alone. Such vulnerability analysis can provide a basis for risk assessment onto which current climate and hydrological projections can be mapped, compared, and updated, if necessary. This can potentially facilitate the communication of the modeling outcomes with the public and other stakeholders. In a similar attempt, *Reynard et al*. [2009] explored U.K. flood risk conditioned on future possibilities for U.K. precipitation using a simple two-parameter sensitivity analysis. This was based on an analysis of the general properties of climate scenarios derived from a range of climate models. The two parameters that were identified were the change in the mean value of daily precipitation and the change in its seasonality. While this is clearly a gross oversimplification of potential changes in future climate, the reduction of the problem to this level provided a powerful visualization of vulnerability onto which the projections from the current generation of regional climate model and GCM could be mapped and compared. In this paper, we extend this idea to the direct analysis of streamflow. We develop a generic stochastic framework to reconstruct the potential changes in the historical hydrographs, with which the vulnerability of water resources systems to the changing hydrograph properties can be analyzed. The suggested reconstruction scheme can be considered as an extension of simple annual resampling [e.g., *Potter and Lettenmaier*, 1990] and the *delta*-method [e.g., *Hay et al*., 2000] commonly used in climate change assessment studies. In simple annual resampling, the annual hydrographs are disjointed, shuffled, and randomly rearranged with or without replacement, while the subannual flow quantities remain the same as the historical hydrographs. Here, it is tried to also sample the subannual streamflows using their empirical properties in a way that the temporal dependence structure within the annual hydrographs is preserved. Moreover, in contrast to the conventional delta-method, here, the shifts are directly imposed to the probability and/or timing distribution functions of the streamflow rather than the observed climate variables or their probability distributions [e.g., *Prudhomme et al*., 2002; *Diaz-Nieto* and *Wilby*, 2005; *Elsner et al*., 2010]. We apply the proposed reconstruction algorithm along with the concept of vulnerability maps to assess the response of a real-world water resources system in the Canadian prairies to possible changes in the flow regime.

2. Methodology and the Proposed Reconstruction Scheme

2.1. Rationale

[6] The responses of natural flows to climate variability in snow-dominated regions have been mainly observed in the forms of shifts in the timing of the seasonal flow peak and the expectation of the annual flow volume [*Barnett et al*., 2005]. These two characteristics also have major effects on the performance of the water resources systems in such places. Put simply, the annual volume reflects the total water available to meet the demands; therefore, any decline in the annual volume may be translated into a deficit for one or more user groups, depending on the severity of shortage. A shift in the timing of the annual peak can also cause difficulties in matching the available water with various demands, particularly for the agricultural sector during a short growing season. Accordingly, if these principal characteristics, namely, the expected annual volume and timing of the annual peak, can be effectively represented, then by synthesizing a large and long enough ensemble of flow series, based on different combinations of these primary parameters, an assessment of system vulnerability can be made with respect to the potential changes in the flow regime. Here, we suggest a modular framework, comprising a stochastic scheme to represent, perturb, and reconstruct the flow hydrograph based on the two principal characteristics, which is further linked to a water resources system model to quantify the response of the systems to the reconstructed flow series. In this paper, we used quantile mapping [e.g., *Li et al*., 2010] to independently represent the shifts in the flow characteristics. By considering these key characteristics as two independent random variables, the copula methodology [e.g., *Genest* and *Favre*, 2007] was used to further combine

these shifts in a stochastic manner while maintaining the temporal dependence within streamflow hydrographs.

2.2. Representing and Perturbing the Annual Flow Volume

[7] Considering n years of historical streamflow data at point P, the flow volume for each year $i : i = 1, 2, \ldots, n$ can be approximated as $V_i = \sum_{j=1}^{m} \text{Flow}_{ij}\Delta_j$, in which Flow_{ij} is the flow rate at the subannual time step $j : j = 1, 2, \ldots, m$ in year i and Δ_j is the duration of time step j. if the time steps are fine and uniform, the historical expectation of the annual volume can be approximated as follows:

$$E(V) = \frac{\Delta}{n}\sum_{i=1}^{n}\sum_{j=1}^{m}\text{Flow}_{ij} = \Delta\sum_{j=1}^{m}\frac{\sum_{i=1}^{n}\text{Flow}_{ij}}{n} = \Delta\sum_{j=1}^{m}E(\text{Flow}_j), \tag{1}$$

i.e., the expectation of the annual volume can be equally described by the sum of the historical flow expectations at each time step. Based on the central value theory, if the flow at each subannual step a, $1 \le a \le n$ is randomly sampled using the cumulative distribution function (CDF) of the historical flow data at that time step, then the expectation of the sampled flow would be equal to the historical mean value. Now, consider an arbitrary year T, where $V_T = xE(V)$ and x is the volumetric shift factor. If the relative change in expected annual volume is proportionally distributed across all subannual time steps, then:

$$V_T = \Delta\sum_{j=1}^{m}xE(\text{Flow}_j). \tag{2}$$

[8] This can similarly be simulated by random sampling, using an updated CDF to characterize the flow quantiles after imposing the volumetric shift factor x. Here, we use quantile mapping to update the original flow quantiles at each time step a based on the shift factor x and the historical flow distribution. In quantile mapping, the original random sample z with the CDF F_Z is transformed to a new random sample y with CDF F_Y using the following expression [*Panofsky* and *Brier*, 1963]:

$$y = F_Y^{-1}(F_Z(z)). \tag{3}$$

[9] Based on equation (2), the updated CDF is required to have a new expected value $xE(\text{Flow}_j)$. For applying quantile mapping, two assumptions are made. The first is that the empirical flow range at each subannual time step remains unchanged after the shift in the mean value (an assumption that could be relaxed to accommodate new information concerning nonstationarity of extremes—see later discussion). This means that the highest and the lowest quantiles remain unchanged as the results of the shift in the mean value. Second, we assume that the shift in other flow quantiles conditioned on the shift in the mean value can be mapped by the shift in the quantiles of a normal probability distribution function (PDF; with the same mean and variance as the actual flow data) when it is uniformly displaced. By making these two assumptions and considering the nonexceedance probability $u, u \in [0, 1]$, the updated flow quantile at each time step a, $a = 1, 2, \ldots, m$ can be approximated as the following:

$$\text{Flow}_a^*(u|x) = F_a^{-1}\left(N_{E(\text{Flow}_a),\sigma(\text{Flow}_a)}\left\{N^{-1}{}_{E(\text{Flow}_a),\sigma(\text{Flow}_a)}(u)\right\}\right), \tag{4}$$

where $E(\text{Flow}_a)$ and $\sigma(\text{Flow}_a)$ are the mean and standard deviation of the historical flow values at time step a, respectively, $\text{Flow}_a^*(u|x)$ is the updated flow corresponding to the nonexceedance probability u and shift factor x, N is the CDF of the standard normal distribution with mean zero and variance one; and finally, N^{-1} and F_a^{-1} are the inverse CDFs of the standard normal distribution as well as the historical flow at time step a. Figure 1 demonstrates a hypothetical application of the proposed procedure. Figure 1a explains the example, assuming arbitrarily that the expected flow at time step i is decreased by 25% ($x = 0.75$). Also, the black, blue, and red lines show the PDFs of the historical flow as well as the considered normal distribution before and after the shift, respectively. Figure 1b shows how the idea of quantile mapping was implemented to update the historical flow quantiles. Also, the black, blue, and red lines show the empirical CDFs of the historical flow as well as the normal distribution before and after the shift, respectively. By applying equation (4), the updated flow quantiles can be sampled using a large set of random numbers (gray line). It should be noted that the flow quantiles are updated using the inverse CDF of the historical flow (F_a^{-1}); therefore, the general

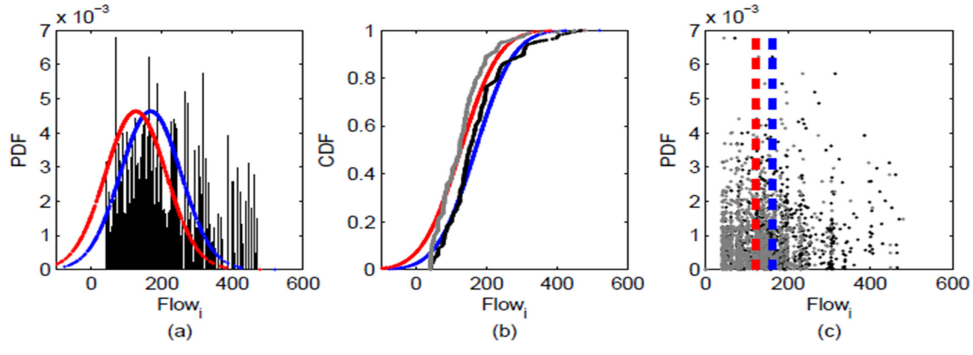

Figure 1. The suggested method for shifting the flow distribution at each subannual time step using quantile mapping: (a) conceptualization, (b) implementation of quantile mapping, and (c) the shifted (gray) versus actual flow (black) distributions as well as their expected values before (blue) and after (red) the shift.

characteristics of the flow CDF such as the domain and the upper skewness are maintained after the shift. In Figure 1c, the flow distributions before (black) and after (gray) the shift are compared. Comparing the expected values of the original (blue; 162.5 CMS (cubic meter per second)) and shifted flow expectations (red; 122.3 CMS) shows that the desired shift can be efficiently imposed on the historical flow by the suggested method.

[10] Figure 2 shows how the proposed mechanism can update the flow distributions at every subannual time step, a way that the expected annual volume shifts as desired. In Figure 2a, the black line shows the expected annual hydrograph, and the boxplots show the historical flow distribution at every weekly time step. In all boxplots, the blue boxes represent the interval between Q25 and Q75, the whiskers cover the regions between ± 2.7 times of the standard deviations, and the red crosses show the remaining outliers. This setting was used throughout this paper.

[11] Figures 2b–2d show the reconstructed flow distributions when the expected annual volume has no change, 25% decline, and 25% incline, respectively. In Figure 2, the green lines represent the expected annual hydrographs, and the boxplots show the reconstructed flow distributions after imposing the shift. Comparing the historical with the reconstructed flow distributions (Figures 2b–2d) demonstrates how the proposed method shifts the weekly flow distributions upward or downward to represent the desired shift in the expected annual flow volume.

2.3. Representing and Perturbing the Timing of the Peak

[12] Here, we suggest a modified version of quantile mapping to shift the timing of the annual peak. To do so, the annual flow hydrograph should be first translated into a cumulative time distribution function (TDF). TDF represents the ratio of the total annual volume, passed prior to or at each subannual time step. Considering subannual time step $a : a = 1, 2, \ldots, m$ and assuming uniform time steps with duration Δ across a year, the TDF can be defined at the time step a as

$$\mathrm{TDF}(a) = \frac{\sum_{i=1}^{a} \mathrm{Flow}_i}{\sum_{j=1}^{m} \mathrm{Flow}_j}, \tag{5}$$

where Flow_i is the flow at the time step i. TDF has the same characteristics as probabilistic CDF; therefore, if the total annual volume and the TDF are known, then the flow at each time step can be approximated using

$$\mathrm{Flow}_a = \{\mathrm{TDF}(a) - \mathrm{TDF}(a-1)\} \sum_{j=1}^{m} \mathrm{Flow}_j. \tag{6}$$

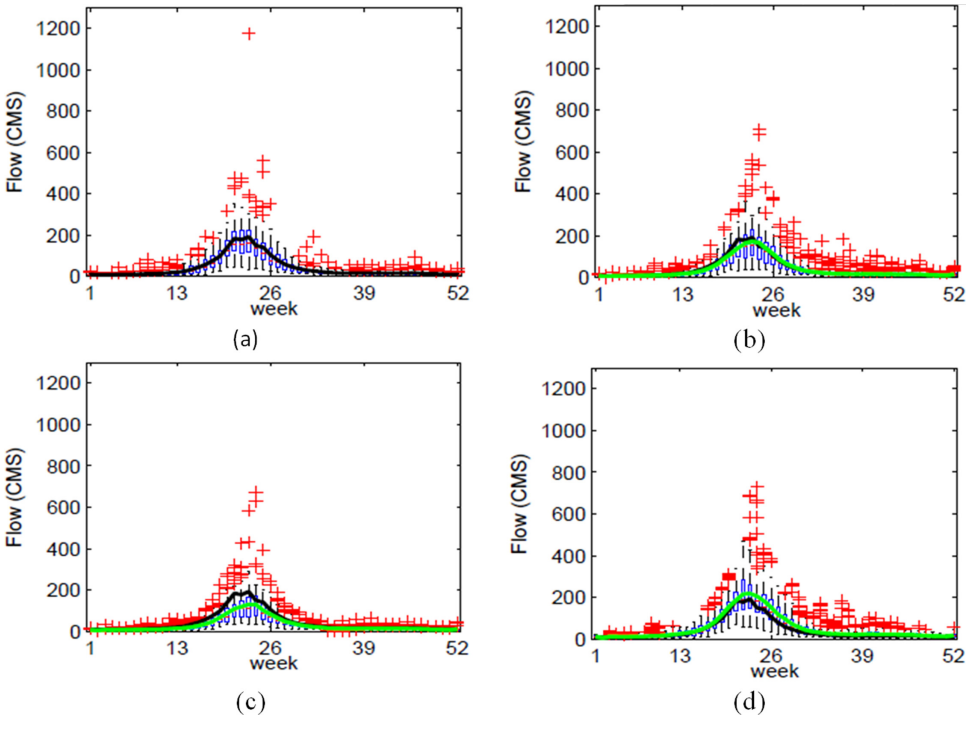

Figure 2. Reconstructing the weekly flow distributions with the desired shift in the expected annual volume using the suggested approach: (a) historical weekly flow distributions when compared with reconstructed weekly flow distributions considering, (b) no change in the expected annual volume, (c) 25% decline in the expected annual volume, and (d) 25% incline in the expected annual volume. The black and the green lines are the expected annual hydrographs based on the observed and the reconstructed distributions, respectively.

[13] As the peak shifts, the TDF should also change at every time step. Here, we assumed that the instantaneous displacements in the TDF are linearly scaled with respect to the time of peak. This implies that the TDF should have the maximum shift at the time of peak and zero shifts at the beginning and the end of the annual flow hydrograph. This can be conceptualized using the displacement of a triangular mapping function for which the apex shows the peak before and after the desired shift, while the base points remain unchanged. Figure 3 illustrates the proposed conceptualization. Figure 3a describes an example, in which it is arbitrarily desired that the peak of the annual flow (black line) shifts 4 weeks earlier. The blue and red lines show the triangular mapping function before and after the shift. Figure 3b shows how the modified version of quantile mapping can be implemented in this case. The black, blue, and red lines show the TDFs of the actual annual hydrograph as well as the triangular annual hydrographs before and after the desired shift, respectively. In this juncture, the shifted TDF (gray line) at each time step a can be approximated as

$$\mathrm{TDF}_{\mathrm{shifted}}(a) = \mathrm{TDF}_{\mathrm{original}}(a) - \mathrm{TDF}_{\mathrm{tri1}}(a) + \mathrm{TDF}_{\mathrm{tri2}}(a), \quad (7)$$

where $\mathrm{TDF}_{\mathrm{shifted}}(a), \mathrm{TDF}_{\mathrm{original}}(a), \mathrm{TDF}_{\mathrm{tri1}}(a), \mathrm{TDF}_{\mathrm{tri2}}(a)$ are the TDFs for the shifted and the original annual hydrographs, as well as the initial and shifted triangular hydrographs, respectively. The shifted TDF can be translated back into the shifted annual hydrograph using equation (6). Figure 3c compares the shifted (gray) and the original (black) annual hydrographs.

[14] Using the above procedure, the flow distribution at every subannual time step can be updated. Figure 4 illustrates an application example. Similar to Figure 2, the black and green lines show the expected annual hydrographs based on the observed and the reconstructed hydrographs, respectively, and the boxplots show the weekly flow distributions. Figures 4a and 4b show the updated distributions, when the expected timing of the peak occurs 4 weeks earlier and 4 weeks later, respectively. Figure 4 demonstrates how the proposed method shifts the expected annual hydrograph to the left or right to represent the desired shift in the expected annual peak time. The expected shifts in the timing of the peak can be imposed on the expected annual hydrograph with only 0.4 and −0.6 weeks error in reconstruction (Figures 4a and 4b, respectively). As the updated TDFs are translated into the flow hydrographs using the estimated annual volume for each year (equation (6)), the total annual volume should be maintained after the shift. The expected values for annual volume in Figures 4a and 4b are 99% and 98%, respectively, of the historical expected annual volume, showing slight errors in preservation of the annual volume.

2.4. Representing the Temporal Dependence Structure

[15] The temporal correlation structure within annual flow hydrographs should be maintained during the flow reconstruction. Here, we used copula methodology to estimate the conditional probabilities of flow at every time step, given the flow at the previous step. In brief, if u and v are two continuous random variables with marginal CDFs of $F_U(u)$ and $F_V(v)$, the joint cumulative distribution of $F_{U,V}(u, v)$ can be described as [*Sklar*, 1959]:

$$F_{U,V}(u,v) = C(u^*, v^*), \text{ where } u, v \in R \text{ and } u^* = F_X(u), \quad v^* = F_Y(v) \quad (8)$$

[16] C is the copula function. By sampling two uniform random numbers u^* and v^*, the flow at each time step i can be sampled using the procedure outlined by *Salvadori* and *De Michele* [2007]:

$$\begin{aligned} \mathrm{Flow}_i^* &= F_i^{-1}\left\{C_{u^*}^{-1}(v^*)\right\}, \text{ and} \\ C_{u^*}(v^*) &= \mathrm{P}\left\{F_i(\mathrm{Flow}_i) \le v \,|\, F_{i-1}\left(\mathrm{Flow}_{i-1}^*\right) = u^*\right\} \\ &= \frac{\partial}{\partial u} C_{i,i-1}(u^*, v^*), \end{aligned} \quad (9)$$

where Flow_i^* is the sampled flow at time step i, Flow_{i-1}^* is the sampled flow at time step $i-1$, F_i and F_{i-1} are the marginal flow CDFs at time steps i and $i-1$, $C_{i,i-1}$ is the parametric copula structure, linking the flow CDFs at time steps i and $i-1$, and P is the conditional CDF. Figure 5 shows how the application of a cascade of copula models can improve the preservation of the observed weekly correlation matrix and smoother annual hydrographs in two successive years. In this example, empirical marginal distributions and Gaussian copulas were used for flow sampling. The Gaussian copula can be formulated as the following [*Nelsen*, 2006]:

$$C^{\mathrm{Gaussian}}(u,v) = \Phi_\Sigma\left(\phi^{-1}(u), \phi^{-1}(v)\right), \quad (10)$$

where ϕ^{-1} is the standard normal distribution $N(0,1)$ and Φ_Σ is the multivariate normal distribution with mean 0 and

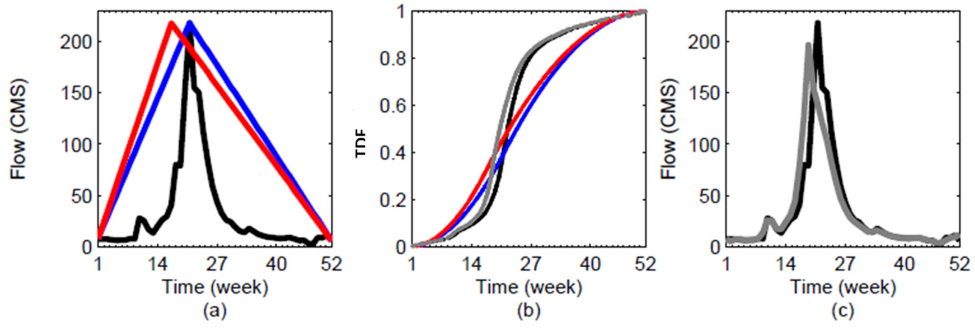

Figure 3. The proposed method for shifting the time of the peak: (a) conceptualization, (b) implementation of quantile mapping, and (c) shifted versus actual hydrographs.

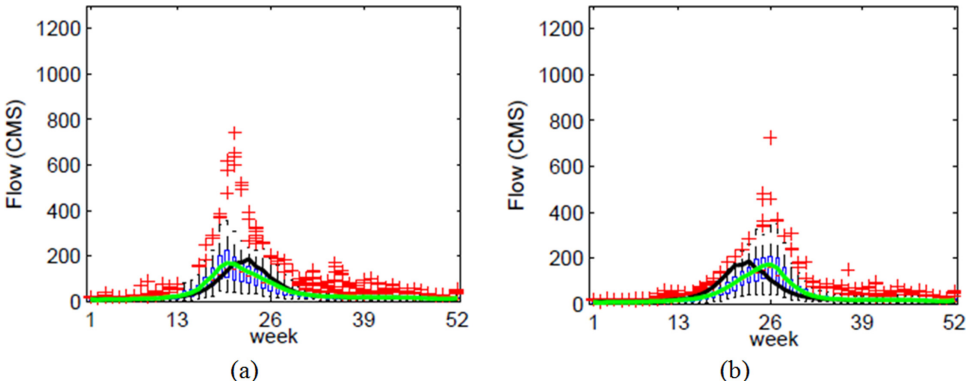

Figure 4. Reconstructing the weekly flow distributions with the desired shift in the expected timing of the annual peak: (a) 4 weeks earlier expectation of the annual peak; and (b) 4 weeks delay in the annual peak. In Figures 4(a) and 4(b), the black and green lines refer to expected annual hydrographs based on the observed and the reconstructed distributions, respectively.

covariance matrix Σ. The maximum likelihood method was used to estimate the parameters of the copula models. Potentially, several joint and marginal distributions can be used instead of the Gaussian copula and empirical margins. Apart from the Gaussian copula introduced in equation (10), two other bivariate structures from the family of Archimedean copulas, namely, Clayton and Frank, were also considered for linking the flow at each time step to the reconstructed flow at the previous time step. Considering, two random variates u and v, which can be taken as the marginal CDF values according to equation (8), Clayton and Frank copulas can be described as [*Nelsen*, 2006]:

$$C_{\theta}^{\text{Clayton}}(u,v) = \left(u^{-\theta} + v^{-\theta} - 1\right)^{-1/\theta}, \tag{11}$$

$$C_{\theta}^{\text{Frank}}(u,v) = \frac{1}{\theta}\log\left[1 + \frac{\left(e^{-\theta u} - 1\right)\left(e^{-\theta v} - 1\right)}{\left(e^{-\theta} - 1\right)}\right], \tag{12}$$

where θ is the copula parameter in both equations. The effects of different copula and marginal quantifications on

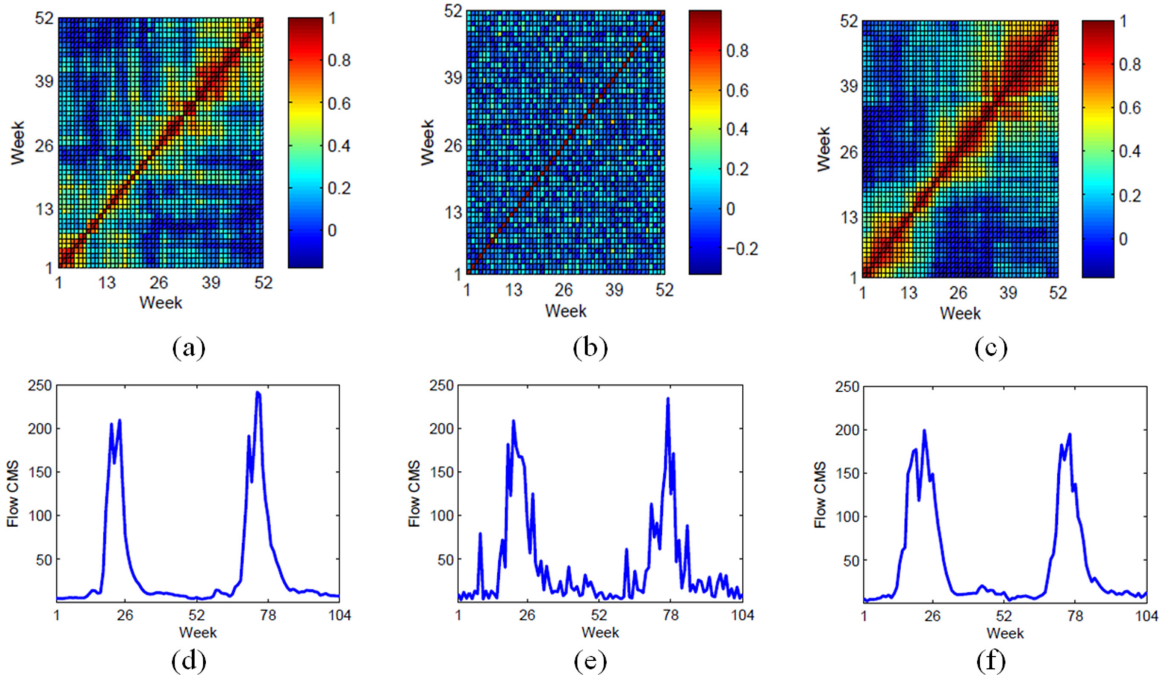

Figure 5. Comparison among the observed, independently reconstructed, and copula-based reconstructed flow hydrographs in terms of preserving the temporal dependence structure and the shape of the reconstructed hydrographs: (a) historical correlation matrix, (b) independently reconstructed correlation matrix, (c) copula-based reconstructed correlation matrix, as well as two successive (d) historical flow hydrographs, (e) independently reconstructed flow hydrograph, and (f) copula-based reconstructed flow hydrograph. In Figures 5a–5c, the correlation matrices are shaded using the color scheme shown in the sidebars.

the quality of reconstruction will be discussed in more detail in section 4.1.

2.5. Proposed Single-Site Reconstruction Algorithm

[17] The introduced procedures for representing and perturbing the annual flow volume and the timing of the peak can be combined in a unified sampling framework to reconstruct the annual flow hydrographs with the desired shifts at any point on the river network for which flow data exist. Before flow reconstruction, the desired shifts in the annual volume and timing of the peak should be set during the course of simulation. The reconstruction scheme can be summarized as

[18] 1. Obtain the TDFs for all the available annual hydrographs.

[19] 2. Perturb the TDF of each historical annual hydrograph given the desired shift in the timing of the peak and the procedure outlined in section 2.3.

[20] 3. Translate the perturbed TDFs into annual flow hydrographs and, consequently, obtain the perturbed empirical flow distributions at each subannual time step.

[21] 4. Update the perturbed empirical flow distributions given the volumetric shift factor and the procedure introduced in section 2.2.

[22] 5. Sample a uniform random number u_1 between 0 and 1.

[23] 6. For every time steps $i : 2 \leq i \leq m$ (m is the number of time step within a year):

Select an appropriate distribution for marginal quantification.
Select a suitable copula structure for describing the conditional probabilities at the time steps i and $i-1$.
Find the parameters of the marginal CDFs at the time steps i and $i-1$. Accordingly, find the parameters of the copula structure.
Sample a uniform random number v between 0 and 1.
Find $u_i = C^{-1}_{ui-1}(v)$.
If $i = 2$ find $\text{Flow}_1 = F_1^{-1}(u_1)$.
Find $\text{Flow}_i = F_i^{-1}(u_i)$.

[24] 7. Repeat steps 5 and 6 until the desired number of realizations is obtained.

[25] 8. Repeat steps 1–7 until the desired number of simulation years is obtained.

3. Case Study

3.1. South Saskatchewan River Basin

[26] The South Saskatchewan River Basin (SSRB) is a transjurisdictional river, located in a semiarid cold continental region with significant variability of climate in time and space. The SSRB is subject to an interprovincial apportionment agreement as it moves from southern Alberta into Saskatchewan, which in essence requires Alberta to pass 50% of its natural water supply to Saskatchewan every year. Snow (and glacier) melts in the Rocky Mountains are the major sources of water supply in SSRB. Roughly, 90% of the total river flow comes from the Rocky Mountains in Alberta [*Pomeroy et al*., 2005]. Important changes have been observed in the Rocky Mountains, associated with warming temperatures, including retreating glaciers, smaller snowpacks, earlier spring snowmelt and reduced streamflow [e.g., *Comeau et al*., 2009]. These are expected to affect the annual streamflow, possibly with large declines in summer runoff. This can increase the chance of severe droughts [*Lemman et al*., 2007]. The SSRB in Alberta has three major tributaries, the Red Deer, the Bow, and the Oldman rivers. The Red Deer system is the largest in area (≈46,000 km^2) with the lowest mean annual flow volume (1665 MCM (million cubic meter)), compared to the Bow (≈25,000 km^2; 3841 MCM) and the Oldman (≈28,000 km^2; 3291 MCM). This is due to the low proportion of the mountainous area in the Red Deer basin [*Martz et al*., 2007]. The SSRB in Alberta supports a complex water resource system, with roughly 11,000 licensees, grouped into around 500 policy clusters with individual rule curves and demand characteristics [*Alberta Environment*, 2010]. Figure 6 shows a simplified schematic of the water resources system in southern Alberta, with the major subsystems and the linkage among them.

[27] Flow regulation and extensive water use have had significant impacts on the flow in both the Bow and the Oldman rivers. For instance, winter flows have significantly increased in the Bow river due to winter releases from series of hydroelectric reservoirs owned by Trans Alta Utility. Although the water use is quite diverse in southern Alberta, diversions for irrigated agriculture account for almost 88% of the total withdrawal ignoring the possible return flows into the system [*Martz et al*., 2007].

3.2. Water Resources Management Model

[28] Alberta Environment uses the Water Resources Management Model [WRMM; *Alberta Environment*, 2002] to simulate the behavior of the water resources system in southern Alberta. WRMM is a simulation model that optimally allocates the water to the competing demands given the state of the system and the operational policies. The water allocation in WRMM is based on linear programming. The model has been implemented frequently to characterize the response

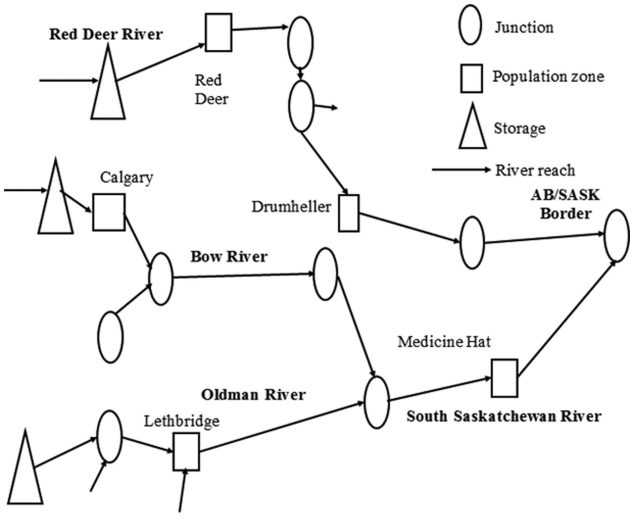

Figure 6. A simplified schematic of the SSRB water resources system in southern Alberta from (left) the Rocky Mountains headwaters to (right) Saskatchewan border.

of the system to different natural conditions and planning alternatives. The latest version of the WRMM model for southern Alberta was used in this study [*Alberta Environment*, 2010]. The key inputs to the model are historical streamflow data in southern Alberta, irrigation demands and the corresponding return flows, nonirrigation withdrawals, reservoir and canal capacities, license priorities, operating policies, in-stream flow needs, water conservation objectives (WCOs), and the interprovincial apportionment requirements. In-stream flow needs generally include minimum flow requirement or so-called fish rule curves that characterize the water demand for aquatic habitats based on the flow quantity/quality as well as the time of the year. WCOs are more recent practices in some part of the system. In simple terms, WCOs can be considered as the greater of in-stream flow needs and a fraction of instantaneous flow quantity at certain reaches of the system. The period of 1928–2001 with weekly steps was used in this study.

3.3. Selection of the Reference Inflows

[29] Our study focuses on 20 major inflows, accounting for nearly 97% of the total water supply in this system (Figure 7a). The inflows are labeled based on their contribution to the expected annual water supply from the largest (ID 1) to smallest (ID 20). Analyzing the annual autocorrelation revealed that the interannual dependency can be ignored in the considered flows.

[30] Figure 7b shows an analysis of the spatial dependence among the 20 considered inflows in southern Alberta, based on a hierarchical clustering method [*Johnson*, 1967]. In brief, one minus the linear correlation coefficient was used as the distance measure to cluster the data into binary groups. Links show the linear correlation among the inflows, where a shorter link represents a stronger correlation. Based on Figure 7, the inflows can be grouped into three clusters. The first two clusters from the left side describe the dependence among the inflows in the Red Deer and the Oldman sub-basins. The third cluster includes inflows with weaker dependencies. These inflows are 2 (Bow river below Ghost dam), 15 (Highwood river at Mouth), 18 (Belly river at Mouth), and 19 (Elbow river below Glenmore). This is not surprising. Inflows 2 and 15 are the outputs from separate models, entering the Bow system from Trans Alta Utility facilities and the Highwood Irrigation system, respectively. Inflow 18 is a highly regulated inflow entering the Oldman system from the Belly river system. Finally, inflow 19 is the only natural inflow in the Bow river system. The spatial dependences observed in Red Deer and Oldman subbasins should be regarded and maintained in the flow reconstruction. Here, we implemented a simple deterministic approach using linear regression to maintain the spatial correlation structures in these basins. The choice of linear regression was due to its simplicity and the existence of the strong Pearson correlation matrices between the flows in the Oldman and the Red Deer basins. In brief, the weekly streamflow time series for the largest inflows in the Red Deer and the Oldman basins, i.e., inflows 3 (Red Deer river near Jenner) and 1 (Oldman river near Lethbridge) were considered as the primary inflow in each cluster. The primary inflows were independently reconstructed using the above reconstruction algorithm. These inflows were used as the reference time series to reconstruct the other inflows in each sub-basin using an ensemble of linear regression models, which describe the historical weekly linkages between the primary inflow and other inflows in each cluster. Apart from the two major inflows in the Red Deer and the Oldman systems, the other four inflows concentrated in the third cluster were also reconstructed independently. The six independently reconstructed flows can be considered as reference inflows to diagnose the performance of the proposed single-site algorithm.

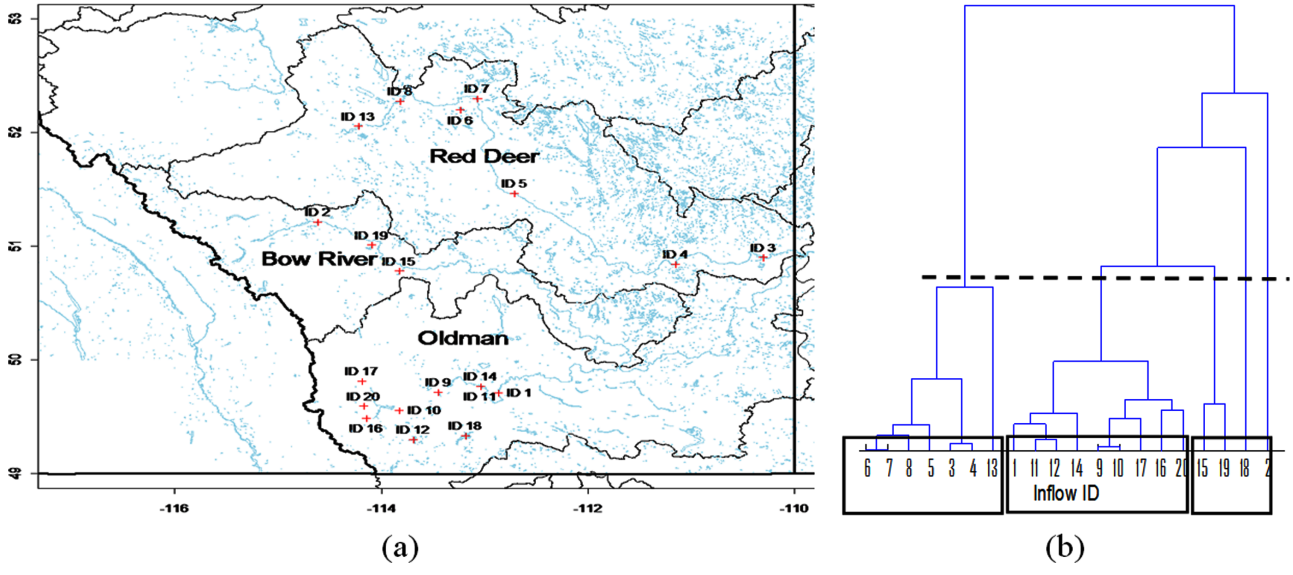

Figure 7. South Saskatchewan River Basin (SSRB) in southern Alberta, Canada: (a) the 20 major inflows considered in this study and (b) the spatial dependence structure among these inflows obtained using hierarchical clustering. The inflows are labeled from largest (ID 1) to smallest (ID 20) according to their portion in the long-term annual supply, averaged over 1928–2001. The dashed line groups the inflows into three clusters.

4. Diagnostic Tests and Scenario Generation

4.1. Calibration and Validation of the Proposed Single-Site Reconstruction Algorithm

[31] Considering the six reference inflows in the system, an attempt was made to analyze the effect of different marginal and copula structures on the quality of flow reconstruction. Three marginal options, namely, empirical, empirical with Pareto tails, and gamma distributions, were considered for marginal quantification. Considering the nine different combinations of the selected copula models (equations (10)–(12)) and the three marginal distributions, we ran an experimental study aiming at reconstructing the same flow characteristics, namely, the time of annual peak, the annual volume, and the temporal dependence structure, as the expected historical values during 1928–2001. The maximum likelihood method was used to estimate the parameters of parametric marginal distributions and copula structures. The results revealed that the quality of reconstruction of the expected annual volume and the time of peak does not change among the nine considered configurations. In fact, all nine configurations were able to reconstruct the expected annual volume with less than 5% error in the six reference inflows. The expected errors in representing the time of peak were also found to be marginal (less than a week) in all the configuration/inflow cases. However, some differences emerged in representing the temporal correlation matrix. It was discovered that the errors, contributed from fitted marginal distributions, can result in distortion of the temporal dependence structure after reconstruction. Figure 8 compares the historical weekly correlation matrix (Figure 8a) against the reconstructed correlation matrices obtained using an ensemble of Gaussian copulas, linking empirical (Figure 8b), Pareto tails (Figure 8c), and gamma (Figure 8d) marginal CDFs in the 52 weeks. Figure 8b can resemble the error contributed only by the Gaussian copulas as margins are quantified using the empirical distributions. By the use of Pareto tails distributions for margins, new errors are introduced due to the errors in the marginal Pareto tails distributions (Figure 8c). By the use of the gamma distribution, the Gaussian copula becomes incapable of describing the historical pattern in the correlation matrix, due to the considerable marginal errors (Figure 8d). The empirical margins, therefore, are considered for the rest of experiments.

[32] The analysis of scatter plots revealed that the best copula structure for describing the dependency between successive pairs of weeks may alter depending on the time of year. For the sake of simplicity, we tried to choose one copula structure for sampling at each inflow. This selection was based on using a formal test, suggested by *Genest et al*. [2009], in which the test statistics is

$$\hat{T}_n = n \int_{[0,1]^2} \left\{ \hat{C}(u,v) - C_\theta(u,v) \right\}^2 \mathrm{d}\hat{C}(u,v). \tag{13}$$

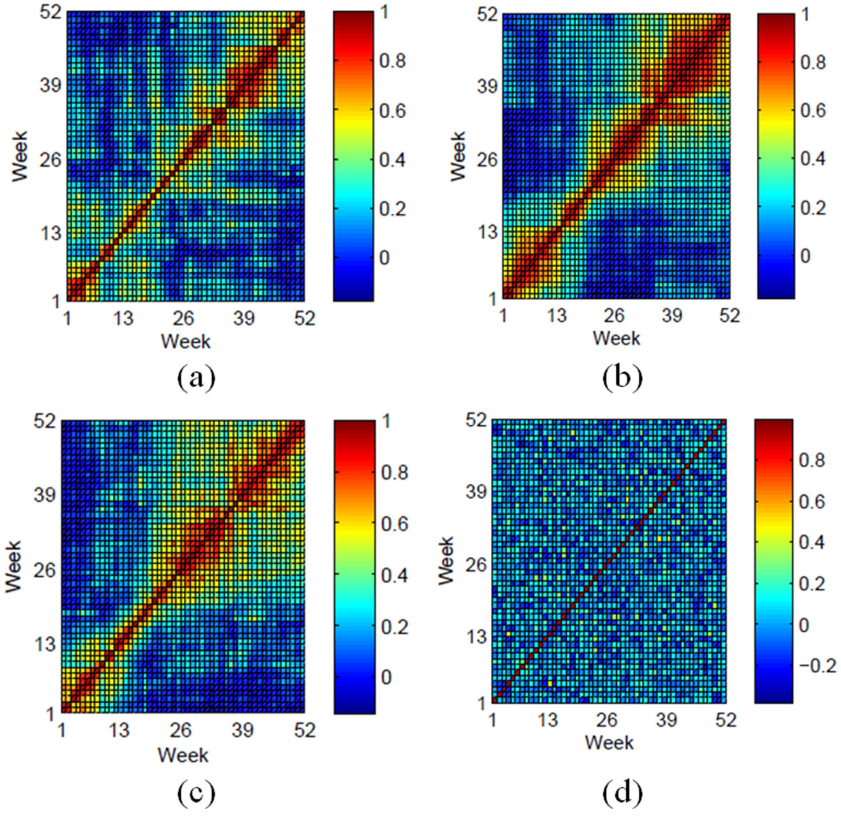

Figure 8. The effect of marginal quantification on the quality of representing the temporal correlation matrix: (a) historical correlation matrix; and the reconstructed correlation matrices using Gaussian copulas linking (b) empirical; (c) Pareto tails; and (d) gamma marginal CDFs. The correlation matrices are shaded according to the sidebars.

[33] Equation (13) measures the distance between the empirical and the fitted parametric copula. In this equation, $\hat{T}_n$ is the test statistics, n is the size of bootstrap sample (74 samples in this study), $\hat{C}(u,v)$ is the empirical copula, and $C_\theta(u,v)$ is the fitted parametric copula. In brief, the three fitted bivariate copulas were used to produce 100 bootstrap sets for every two successive weeks in each of the six reference inflows. Accordingly, the p values were calculated for each pair of successive weeks. Small p values suggest discarding the copula models, whereas large values support its suitability [*Durante* and *Salvadori*, 2010]. Figure 9 compares the expected p values in the six reference inflows using Clayton, Frank, and Gaussian bivariate copulas. The expected p values are estimated by averaging the p values obtained for all pairs of successive weeks in each inflow. Figure 9 clearly shows that the overall efficiency in representing the true temporal dependence structure increases from Clayton to Frank and Gaussian copulas in all six reference inflows. The Gaussian copula, therefore, is chosen for the rest of experiments.

[34] The results obtained, however, are only limited to the reconstruction of the historical flow regime with no shift. Another experimental study, therefore, was performed to validate the proposed reconstruction algorithm using an unseen set of data. We randomly divided the available data for each of the six reference inflows into two portions with 50 and 24 years of data as calibration and validation sets. For each validation year, the shifts in the time of peak and annual volume with respect to the expected values during the calibration phase were extracted. By introducing these parameters to the algorithm, 100 realizations were reconstructed for each validation year using the proposed reconstruction algorithm applied to the calibration set in each inflow. Six different characteristics during the validation years, namely, the expected time of peak, the expected annual volume, the expected weekly correlation matrix, and the expected flow quantiles at 10%, 50%, and 90% nonexceedance levels were considered for further exploration. Figure 10 summarizes the results of this experiment in the six reference inflows. In Figure 10a, the expected time of the peak during 24 validation years (black solid line) is compared with the corresponding value based on 100 reconstructed time series in each reference inflow. The green dots represent the expected time of peak based on 100 reconstructions. For five inflows, the expected reconstructed values have equal or less than ±1 week error. Inflow 18 is the only inflow that exhibits a larger error due to the high interannual variability in the timing of the annual peak, as the result of major upstream regulation. Figures 10b and 10d–10 show the relative errors in reconstructing the expected annual volume as well as the errors in representing the flow quantiles in 10%, 50%, and 90% percentiles, respectively. In Figure 10, the dashed lines highlight the boundary of ±10% error, and the green dots resemble the expected error obtained through 100 realizations. These figures demonstrate the acceptable performance of the proposed reconstruction scheme in representing the expected values of the annual volume as well as the flow quantiles during validation years. In Figure 10c, the overall expected error in reconstructing the weekly correlation matrix is shown. For computing the total expected errors, first, the expected error was computed for each of the six inflows by averaging the errors in 100 realizations. Then, the total expected error was computed by averaging the expected errors obtained for the six reference inflows. The total expected error matrix is shaded according to the color scheme shown in the sidebar. Based on this panel, it can be argued that the temporal dependence during the validation years can be sufficiently described by the Gaussian bivariate copula, with some errors.

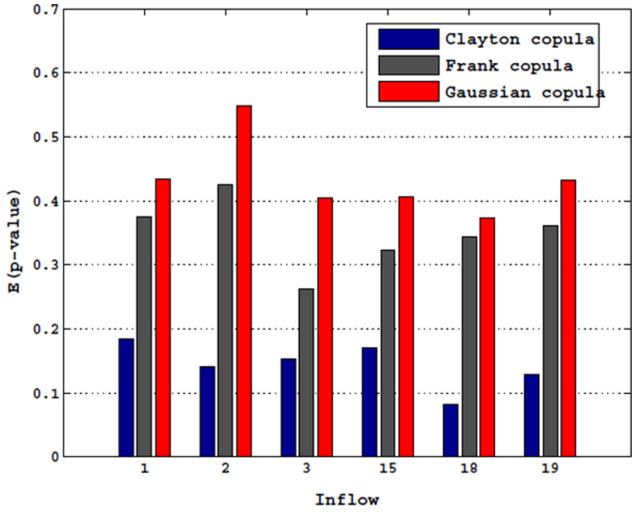

Figure 9. The expected p values, averaged over all successive pairs of weeks based on 100 bootstrap sets, in the six reference inflows.

4.2. Scenario Generation and the Proposed Impact Assessment Study

[35] Having validated the proposed reconstruction algorithm, several scenarios for change in the key flow characteristics can be reconstructed using the historical flow data. Different combinations of these characteristics can provide a diverse ensemble of potential changes in the flow regime. Reconstructing a large number of realizations each with a long simulation period is required to provide the possibility of generating different successions of wet and dry years to portray the possible variabilities within the annual flow hydrographs. The reconstructed records can be further linked to the WRMM model and provide an insight into the response of the water resources system to the shifts in the flow regime. Figure 11 shows an application example, in which five scenarios for shift are considered. This example combines the examples illustrated in Figures 2 and 4. The scenarios characterize the situations where (a) the annual flow is expected to reach to its peak 4 weeks earlier with 25% decline in annual volume; (b) the annual flow is expected to reach to its peak 4 weeks earlier but with 25% increase in the annual volume; and (c) no shift in the annual volume and timing of peak timing or the annual volume is expected. Scenarios (d) and (e) are similar to (a) and (b) but with 4 weeks delay in annual peak timing. For each scenario, 100 realizations were made, each with 74 years of weekly simulation. The first row compares the reconstructed expectation of the timing of the annual peak, with the historical values (black line). The desired shifts are well represented during the reconstruction with an expected error of less than a week. The second row shows the shift

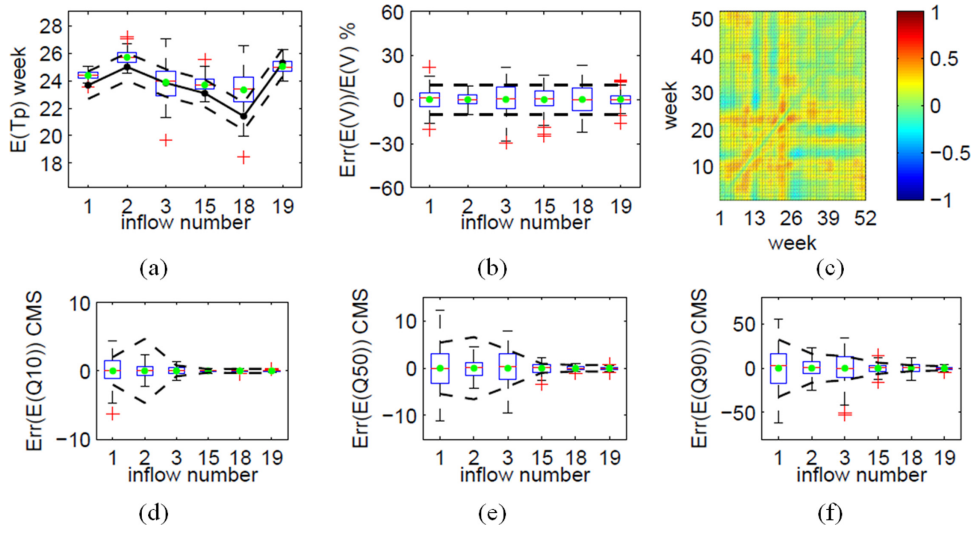

Figure 10. The error in representing the expectation of the flow characteristics in the six reference inflows during the validation phase: (a) historical versus reconstructed expectations for the time of peak, $E(T_p)$, (b) relative error in reconstructing the expected volume, $\mathrm{Err}\{E(V)\}/E(V)$, (c) the expectation of the total error in reconstructing the temporal correlation matrices; as well as the error in reconstruction the expected values of (d) Q10, $\mathrm{Err}\{E(Q10)\}$, (e) Q50, $\mathrm{Err}\{E(Q50)\}$, and (f) Q90, $\mathrm{Err}\{E(Q90)\}$.

in the expectations of the annual volume obtained through 100 realizations. The expected relative error in representing the volume is still quite marginal, staying below 6% for all the considered scenarios. This error seems to be unavoidable, as $\Delta\sum_{j=1}^{m} E(\mathrm{Flow}_j)$ will be the exact expected volume, if $\Delta \to 0$.

[36] The third row shows the expected weekly correlation matrices, averaged over 100 realizations. The matrices are shaded according to the color scheme shown in the sidebar. It can be argued that shifting the timing of the peak not only change the flow distribution at every week but also alters the temporal dependence structure. The last row shows the ensemble of flow-duration curves on a semilogarithmic scale based on 100 realizations for each of the scenarios. The red lines represent the observed flow-duration curves based on the historical weekly data, and the blue lines are the reconstructed flow duration curves obtained based on 100 realizations.

[37] Based on recent climate-change impact assessment studies [e.g., *Martz et al*., 2007; *Alberta Environment*, 2010] and the physical constraints of the flow regime in Alberta, we considered the ranges of ±25% change in the annual volume as well as −5 to +8 weeks shift in the expected timing of the annual peak, gridded using steps of 5% and 1 week, respectively (154 subgrid combinations). For each subgrid, 100 realizations of weekly flow time series were generated with a length of 60 years for the six reference inflows. Inflows 1 and 3 were further used to reconstruct the flow in the other 14 inflows in the Oldman and Red Deer basins (see section 11). The 20 reconstructed inflows were input to the WRMM model of the SSRB in Alberta. We considered the period of 1928–1987 for model simulation. Before running the WRMM model using the reconstructed series, the apportionment requirements, the in-stream flow needs, and WCOs need to be updated for each scenario/realization. We assumed that the in-stream flow needs are solely dependent on the weekly flow quantities through a set of piecewise linear equations, linking the weekly flows to the in-stream needs in natural reaches. Accordingly, we further updated the WCOs in the required reaches based on the relations provided by *Alberta Environment* [2010]. The other components of the WRMM model such as demand remained unchanged. Here, we focused on the variations in the risk of system infeasibility and the variation in the general characteristics of apportionment flow as the result of the considered 154 scenarios of change. In the WRMM definition, system infeasibility represents a condition in which the system state violates the system's physical constraints and/or the system cannot satisfy its minor "must-meet" demands. When the system reaches infeasibility, the model stops and the reason of infeasibility is reported as output [*Alberta Environment*, 2002]. In this study, no attempt was made to adjust the operational policies to satisfy the minor demands or keep the system in its acceptable physical boundaries.

5. Results of Vulnerability Assessment

5.1. Chance of Infeasibility

[38] The chance of infeasibility can be described as the proportion of the total number of WRMM runs (100 runs for each of the 154 scenarios), which stop before completing the whole simulation. In this study, a 50% chance of infeasibility was chosen as the critical threshold. In the absence of any other information (e.g., previous knowledge of the system, water managers' attitude toward risk, etc.), the chances of the system "to reach" or "not to reach" the state of infeasibility are equal (50-50) for every scenario. Therefore, given a particular shift scenario, if the system reaches infeasibility in more than 50% of the realizations, it can be inferred that the applied water allocation policy is likely infeasible and some adaptations are needed to bring the system into the operational mode. Coping conditions,

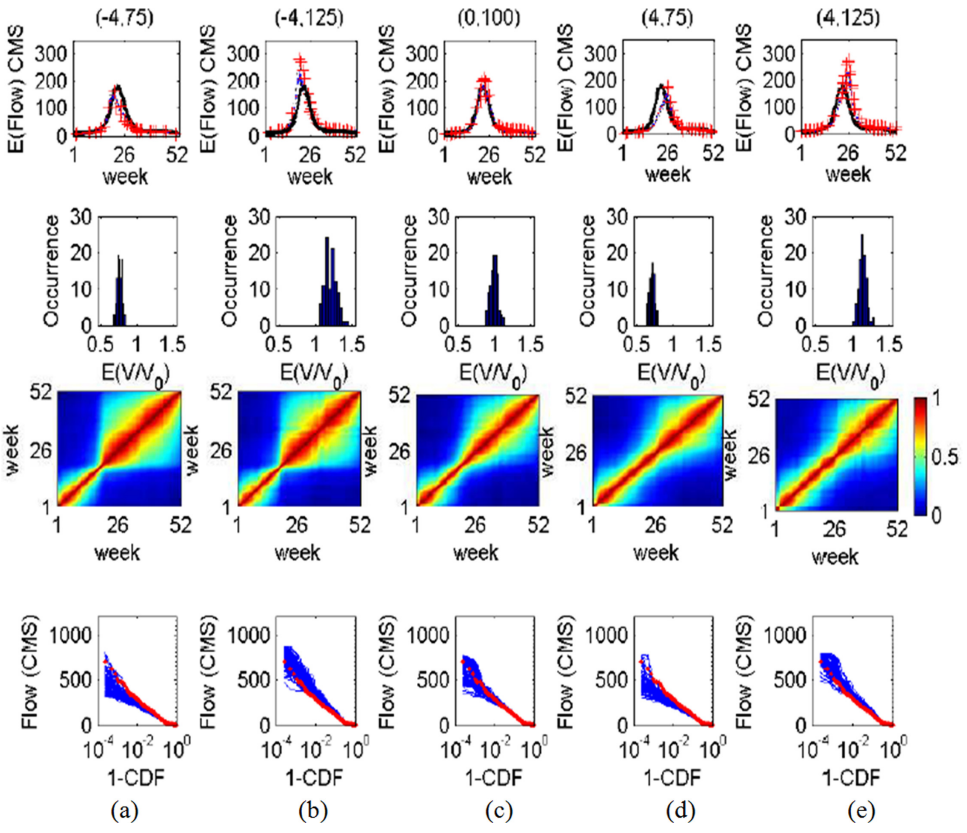

Figure 11. Generating five different flow regimes using the proposed reconstruction algorithm: (a) 4 weeks earlier peak, 25% decline in annual volume, (b) 4 weeks earlier peak, 25% incline in annual volume, (c) no shift in peak time and annual volume, (d) 4 weeks delayed peak, 25% decline in annual volume, and (e) 4 weeks delayed peak, 25% incline in annual volume. The first row compares the historical versus reconstructed expected annual hydrographs. The second row shows the reconstructed shifts in the annual volume. The third row shows the expected weekly correlation matrices, and the last row shows the historical versus reconstructed flow-duration curves. For each scenario, 100 realizations were generated. The correlation matrices are shaded according to the sidebar.

therefore, resemble the scenarios where the chance of infeasibility goes below 50%, showing that despite the possible shortages, the system can likely allocate the must-meet demands and stay within its acceptable physical boundaries throughout a full simulation. It should be noted that, in a more general sense, the choice of the critical threshold is rather arbitrary and any other probability value can be considered to draw the line between coping and infeasibility modes. Figure 12 provides a general picture about the system infeasibility by demonstrating the probability of system infeasibility during the 60 years of simulation.

[39] Although there are some anomalies at the lower right edge of Figure 12, where the limitation in the number of sampled data introduces error in calculation of the probability values, this color chart can provide a powerful graphical insight into the system vulnerability to changes in flow regime. It also can show how gradually the system can approach from feasibility to infeasibility. With only 25% decrease in the expected annual flow volume and more than ± 2 weeks shift in the expected annual flow timing, the system reaches the critical threshold. As would be expected, the majority of infeasibility cases occur when the expected annual volume declines. The system is sensitive to both earlier

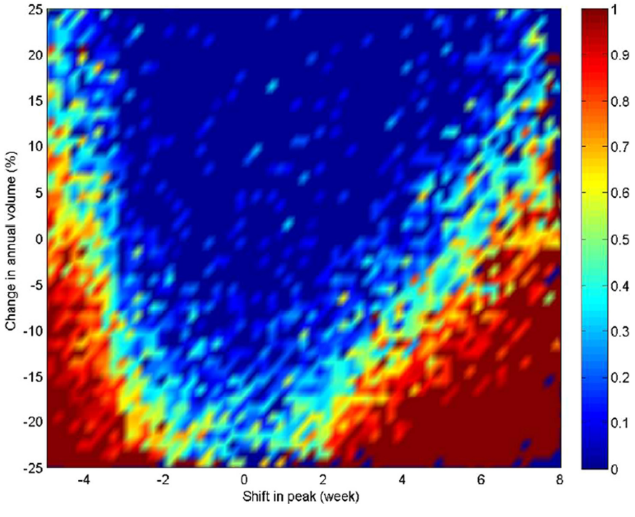

Figure 12. The chance of system infeasibility with respect to the changes in expected annual flow volume and peak timing in southern Alberta. Probabilities are represented according to the color scheme in the sidebar.

and delayed timing of the peak, although it seems that the vulnerability to earlier peak is more severe: Even without any change in the expectation of the annual volume, the system reaches a critical threshold if the peak flow occurs around 1 month earlier. As discussed above, earlier peak and decreased annual volume can be possible cases in the near future, considering earlier melt and decline in the snow packs in the Rocky Mountains due to the warming climate [*Lemman* and *Warren*, 2004; *Lemman et al*., 2007].

5.2. Expectations of the Annual Apportionment

[40] The implementation of 50% natural flow apportionment in the case of shift in the flow regime is a major concern for policy makers in both sides of the provincial borderline. Figure 13 demonstrates the expectations of mean annual flow apportionment during the 60 years of simulation with respect to the considered shifts in the flow regime. The expected values are calculated as the average annual ratio of the Alberta's natural water availability. The blue region represents the conditions in which the system goes into infeasibility with more than 50% chance as defined above (Figure 12). We did not calculate the apportionment statistics in such cases, as the system would require adaptation. The shaded region shows the coping conditions based on the above definition where the chance for infeasibility remains below 50%. Figure 13 clearly demonstrates that on average, Alberta can provide more than 50% of its natural supply to Saskatchewan if the system stays in the coping conditions in southern Alberta. Depending on the scenario/realization, the expected ratio of apportionment (Figure 11c) would be between 53% and 74% of the annual supply during the course of simulation. Our results also show that the variability in the annual apportionment rate increases by positive shifts in annual volume. The annual variability in apportionment rate, however, was found rather independent of the timing of the annual peak.

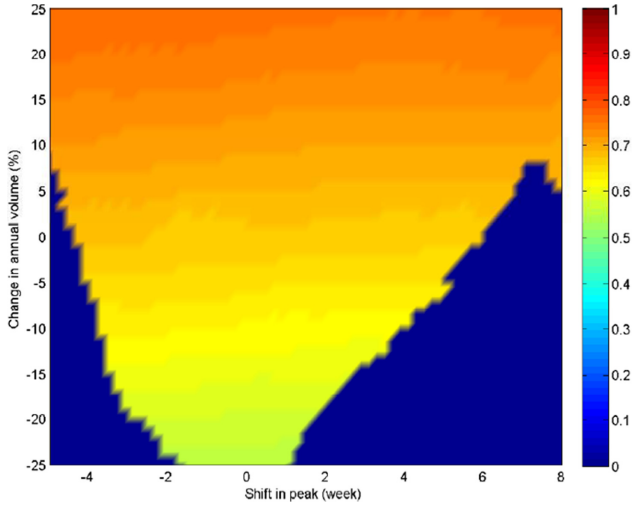

Figure 13. The expected mean for Saskatchewan apportionment under current policies as the ratio of Alberta's natural supply. The blue regions show the conditions in which the system has more than 50% chance to become infeasible during the simulation. The apportionment ratios are represented using the color scheme shown on the sidebars.

6. Summary and Further Remarks

[41] Due to the current limitations in climate and hydrological models, more generic methods are required to address the possible critical conditions in water resources systems due to a range of potential changes in the flow regime. Such vulnerability analysis can go beyond the predictions of climate and hydrological models and can provide a basis for risk assessment onto which the results of current climate and/or hydrological models can be also mapped and compared. Such capabilities can potentially facilitate the communication of the modeling outcomes with public and stakeholders. This paper focused on developing such a framework. We introduced a couple of simple conceptualizations using the idea of quantile mapping to represent and perturb the key characteristics of the annual flow hydrograph, namely, the time of peak and the flow volume. These representations were further combined through a stochastic sampling scheme based on the copula methodology that generates subannual flow values at the local scale with regard to the temporal dependence structure within the observed annual streamflow hydrographs. The proposed single-site reconstruction scheme was verified using six reference streamflows in southern Alberta, Canada. A simple linear regression framework was implemented to maintain the spatial dependence and to transfer the flow from the reference inflows to the other major inflows in the system. The reconstructed flow series were further linked to the WRMM simulation model to map some general aspects of the system response as the function of changes in the expected annual volume and the peak timing. We have realized that the chance of system infeasibility increases with the decrease in the flow volume especially when it is mixed with the earlier timing of the annual peak. The system can likely maintain the interprovincial apportionment commitment if it stays within the coping conditions in Alberta.

[42] Although the proposed single-site reconstruction algorithm was able to represent the general aspects of unseen hydrographs with an acceptable degree of accuracy, several improvements can be made, particularly in conceptualizing the mechanisms of hydrograph change. It should be noted that we have used two very simple conceptualizations for representing the shifts in the timing and the volume of the annual flow. We do not advise that the changes in flow quantiles can be fully mapped by a uniform shift in a normal distribution with no change in empirical flow range at each subannual time step. We also do not claim that a linear shift can wholly represent the mechanism of shift in the time of peak as a triangular distribution function may not appropriately describe the shift in conditions in which the annual hydrograph has two separate peaks corresponding to the spring snowmelt and summer rainfall, respectively. In addition, despite several benefits of central value theory, there is always a fear of missing the most extreme events. As Figure 2b clearly shows, the sampled flow distributions based on 74 years of reconstructions missed the most extreme flood event during the historical record. Attempts are, therefore, required to enhance the sampling flexibility and to improve the marginal quantifications using parametric distributions. This would be necessary for extrapolating beyond the historical flow range at each subannual time

step. More experimentation with copula models is required to improve the representation of the temporal dependencies through the stochastic reconstruction. This can be important as we realized that the best copula structure for describing the successive weekly dependence may change depending on the time of the year.

[43] Preserving the spatial dependence structure among the streamflows series in a river network is crucial, especially if the regional assessment of water resources systems is concerned. In this paper, we tried to maintain this using linear regression due to its simplicity and the existence of strong linear correlation matrices between the streamflows in the Oldman and the Red Deer basins; nonetheless, more general spatial-temporal representations should be developed to incorporate both temporal and spatial dependence structures in a fully stochastic framework. Moreover, the current reconstruction algorithm does not account for interannual dependency within the local streamflows. This is a reasonable assumption for the considered flows in southern Alberta. However, interannual dependency can cause considerable variability in the streamflow series and should be handled through reconstruction, if significant. We note that the identification of critical conditions, solely based on the probability of infeasibility, may provide a crude and rather subjective picture of the potential system vulnerabilities. Water managers' attitude toward risk, practical requirements, and more objective (deficit-based) performance measures can be used to create more informative vulnerability maps with respect to the potential alterations in the regional flow regime. The suggested reconstruction scheme is quite flexible and can be considered as a theoretical extension of the simple annual resampling and/or conventional delta-method. However, from the outlook of water resources systems, it is necessary to investigate the extent to which the vulnerability maps are sensitive to the approach taken for the streamflow generation.

[44] As the final remark, we should clarify that the proposed approach is not advised as a replacement for the use of climate and hydrological models. Quantification of the shifts in flow regime due to climate change and other potential forcings is extremely complicated, and no single method is likely to suffice. In fact, we encourage more effort in fusing the stochastic and model-based vulnerability assessment approaches in a unified framework, for an improved model comparison, scenario generation, and uncertainty assessment. However, the results of this analysis suggest that adaptation strategies will become a necessity in southern Alberta in the near future. This is due to the clear decline in snow accumulation and earlier snowmelt in the Rocky Mountains and the increased water demand, both at the upstream and the downstream of the Alberta-Saskatchewan border as the result of the increasing population and the economic growth in Canadian prairies.

[45] **Acknowledgments.** The authors thank Dave McGee, Tom Tang, and Kent Berg of Alberta Environment for providing the historical weekly flow archive and the WRMM model for southern Alberta. They also provided helpful comments during the preparation of the manuscript that significantly improved the quality of this presentation. The authors also appreciate the extremely constructive and in-depth suggestions provided by the Associate Editor and three anonymous reviewers. Financial support for this project was provided by the Canada Excellence Research Chair in Water Security at the University of Saskatchewan.

References

Alberta Environment (2002), *Water Resources Management Model (WRMM)*, Govt. of Alberta, Edmonton, Alberta. [Available at http://www3.gov.ab.ca/env/water/regions/ssrb/wrmmoutput/WRMM/index.asp.] Accessed 26 May 2012.

Alberta Environment (2010), *South Saskatchewan Regional Plan: Water Quantity and Quality Modelling Results*, Govt. of Alberta, Edmonton, Alberta, 89 pp.

Anagnostopoulos, G. G., D. Koutsoyiannis, A. Christofides, A. Efstratiadis, and N. Mamassis (2010), A comparison of local and aggregated climate model outputs with observed data, *Hydrol. Sci. J.*, *55*(7), 1094–1110, doi:10.1080/02626667.2010.513518.

Barnett, T. P., J. C. Adam, and D. P. Lettenmaier (2005), Potential impacts of a warming climate on water availability in snow-dominated regions, *Nature*, *438*(7066), 303–309, doi:10.1038/nature04141.

Beven, K. (2008), On doing better hydrological science, *Hydrol. Processes*, *22*(5), 3549–3553, doi:10.1002/hyp.

Beven, K. (2011), I believe in climate change but how precautionary do we need to be in planning for the future?, *Hydrol. Processes*, *25*(9), 1517–1520, doi:10.1002/hyp.7939. [Available at http://doi.wiley.com/10.1002/hyp.7939, accessed 10 April 2012.]

Budescu, D. V., S. Broomell, and H.-H. Por (2009), Improving communication of uncertainty in the reports of the intergovernmental panel on climate change, *Psychol. Sci.*, *20*(3), 299–308, doi:10.1111/j.1467-9280.2009.02284.x.

Comeau, L. E. L., A. Pietroniro, and M. N. Demuth (2009), Glacier contribution to the North and South Saskatchewan rivers, *Hydrol. Processes*, *23*(8), 2640–2653, doi:10.1002/hyp.

Diaz-Nieto, J., and R. L. Wilby (2005), A comparison of statistical downscaling and climate change factor methods: Impacts on low flows in the River Thames, United Kingdom, *Clim. Change*, *69*, 245–268.

Durante, F., and G. Salvadori (2010), On the construction of multivariate extreme value models via copulas, *Environmetrics*, *21*, 143–161, doi:10.1002/env.988.

Déry, S. J., and E. F. Wood (2005), Decreasing river discharge in northern Canada, *Geophys. Res. Lett.*, *32*(10), 2–5, doi:10.1029/2005GL022845.

Déry, S. J., K. Stahl, R. D. Moore, P. H. Whitfield, B. Menounos, and J. E. Burford (2009), Detection of runoff timing changes in pluvial, nival, and glacial rivers of western Canada, *Water Resour. Res.*, *45*(4), 1–11, doi:10.1029/2008WR006975.

Elsner, M. M., L. Cuo, N. Voisin, J. S. Deems, A. F. Hamlet, J. A. Vano, K. E. B. Mickelson, S.-Y. Lee, and D. P. Lettenmaier (2010), Implications of 21st century climate change for the hydrology of Washington State, *Clim. Change*, *102*(1–2), 225–260, doi:10.1007/s10584-010-9855-0.

Genest, C., and A.-C. Favre (2007), Everything you always wanted to know about copula modeling but were afraid to ask, *J. Hydrol. Eng.*, *12*(4), 347–368.

Genest, C., B. Rémillard, and D. Beaudoin (2009), Goodness-of-fit tests for copulas: A review and a power study, *Insur. Math. Econ*, *44*(2), 199–213, doi:10.1016/j.insmatheco.2007.10.005.

Hall, J., and C. Murphy (2010), Vulnerability analysis of future public water supply under changing climate conditions: A study of the Moy Catchment, Western Ireland, *Water Resour. Manage.*, *24*(13), 3527–3545, doi:10.1007/s11269-010-9618-8.

Hay, L. E., R. L. Wilby, and G. H. Leavesley (2000), A comparison of delta change and downscaled GCM scenarios for three mountainous basins in the United States, *J. Am. Water Resour. Assoc.*, *36*(2), 387–397.

Johnson, S. C. (1967), Hierarchical clustering schemes, *Psychometrica*, *32*(3), 241–254.

Kundzewicz, Z. W., and E. Z. Stakhiv (2010), Are climate models "ready for prime time" in water resources management applications, or is more research needed?, *Hydrol. Sci. J.*, *55*(7), 1085–1089, doi:10.1080/02626667.2010.513211.

Kundzewicz, Z. W., L. J. Mata, N. Arnell, P. Kabat, and T. Oki (2007), Freshwater resources and their management, in *Climate Change 2007: Impacts, Adaptation and Vulnerability. Contribution of Working Group II to the Fourth Assessment Report of the Intergovernmental Panel on Climate Change*, edited by C. E. Hanson et al., pp. 173–210, Cambridge Univ. Press, Cambridge, U. K.

Leith, N. A., and R. E. Chandler (2010), A framework for interpreting climate model outputs, *J.R. Stat. Soc., Ser. C Appl. Stat.*, *59*(2), 279–296, doi:10.1111/j.1467-9876.2009.00694.x.

Lemman, D. S., and F. J. Warren (2004), *Climate Change Impacts and Adaptation: A Canadian Perspective*, Govt. of Canada, Ottawa, Ontario, 174 pp.

Lemman, D. S., F. J. Warren, J. P. Bruce, B. Lavender, T. D. Prowse, I. J. Walker, C. Dickson, S. Nickels, and E. Wheaton (2007), *From Impacts to Adaptation: Canada in a Changing Climate 2007*, Govt. of Canada, Ottawa, Ontario, 448 pp.

Li, H., J. Sheffield, and E. F. Wood (2010), Bias correction of monthly precipitation and temperature fields from Intergovernmental Panel on Climate Change AR4 models using equidistant quantile matching, *J. Geophys. Res.*, *115*, D10101, doi:10.1029/2009JD012882.

Martz L., J. Bruneauand, and J. T. Rolfe (2007), Assessment of the vulnerability of key water use sectors in the South Saskatchewan River Basin (Alberta and Saskatchewan) to changes in water supply resulting from climate change, *SSRB Final Technical Report*. [Available at http://adaptation.nrcan.gc.ca/projdb/107e.php, accessed 26 May 2012.]

Minville, M., F. Brissette, S. Krau, and R. Leconte (2009), Adaptation to climate change in the management of a Canadian water-resources system exploited for hydropower, *Water Res. Manage.*, *23*(14), 2965–2986, doi:10.1007/s11269-009-9418-1.

Nelsen, R. B. (2006), *An Introduction to Copulas*, Springer, New York.

Panofsky, H. A., and G. W. Brier (1963), *Some Applications of Statistics to Meteorology*, Pennsylvania State Univ., University Park, Pa, 224 pp.

Pielke, R. A., and R. L. Wilby (2012). Regional climate downscaling: What's the point?, *EOS Trans. AGU*, *93*(5), 52–53, doi:10.1029/2012EO050008.

Pomeroy, J. W., D. D. Boer, and L. W. Martz (2005), *Hydrology and Water Resources of Saskatchewan*, Univ. of Saskatchewan, Saskatoon, Saskatchewan, 25 pp.

Potter, K. W., and D. P. Lettenmaier (1990), A comparison of regional flood frequency estimation methods using a resampling method, *Water Resour. Res.*, *26*(3), 415–424, doi:10.1029/WR026i003p00415.

Prudhomme, C., N. Reynard, and S. Crooks (2002), Downscaling of global climate models for flood frequency analysis: Where are we now?, *Hydrol. Processes*, *16*(6), 1137–1150, doi:10.1002/hyp.1054.

Reynard, N. S., S. Crooks, A. L. Kay, and C. Prudhomme (2009), Regionalized impacts of climate change on flood flows, *Joint Defra/EA Flood and Coastal Erosion Risk Management R&D Programme Tech. Rep. FD2020/TR*, Dept. for Environment, Food and Rural Affairs, London, U. K., 113 pp.

Salvadori, G., and C. D. Michele (2007), On the use of copulas in hydrology: Theory and practice, *J. Hydrol. Eng.*, *12*(4), 369–380.

Sklar, A. (1959). Fonctions de repartition a n dimensions et leurs marges, *Inst. Stat. Univ. Paris Publicat.*, *8*(5), 229–231.

Stedman, R. C., D. J. Davidson, and A. Wellstead (2004), Risk and climate change: Perceptions of key policy actors in Canada, *Risk Anal.*, *24*(5), 1395–406, doi:10.1111/j.0272-4332.2004.00534.x.

Swart, R., L. Bernstein, M. Ha-Duong, and A. Petersen (2008), Agreeing to disagree: uncertainty management in assessing climate change, impacts and responses by the IPCC, *Clim. Change*, *92*(1–2), 1–29, doi:10.1007/s10584-008-9444-7.

Viviroli, D., et al. (2010), Climate change and mountain water resources: overview and recommendations for research, management and politics, *Hydrol. Earth Syst. Sci. Discuss.*, *7*(3), 2829–2895, doi:10.5194/hessd-7-2829-2010.

Wheater, H. S. (2009), Water management for a changing climate; challenges and opportunities, paper presented at the 18th Convocation of the International Council of Academies of Engineering and Technological Sciences, Calgary, Alberta.

Wilby, R. L. (2010), Evaluating climate model outputs for hydrological applications, *Hydrol. Sci. J.*, *55*(7), 1090–1093, doi:10.1080/02626667.2010.513212.